processes

MDPI

Article

Solar-Assisted Paraquat Removal Using Coconut-Waste-Derived Biofiber/Carbon/TiO_2 Composites

Nazly G. Chate-Galvis [1], Angélica García-Quintero [1,2] and Manuel Palencia [2,*]

[1] Mindtech Research Group (Mindtech-RG), Mindtech S.A.S, Cali 760032, Colombia; n.chate@mindtech.com.co (N.G.C.-G.); angelica.garcia.quintero@correounivalle.edu.co (A.G.-Q.)
[2] Research Group in Science with Technological Applications (GI-CAT), Department of Chemistry, Faculty of Natural and Exact Sciences, Universidad del Valle, Cali 760032, Colombia
* Correspondence: manuel.palencia@correounivalle.edu.co

Abstract

Although TiO_2/carbon composites and cellulose-supported TiO_2 materials have been investigated for pollutant removal, the integration of distinct fractions of coconut biomass into a single fiber-based hybrid architecture remains comparatively underexplored, particularly for solar-assisted paraquat (PQT) removal. In this study, coir fibers from coconut mesocarp were modified with trichlorovinylsilane (TClVS), impregnated with oxidized carbonaceous material (OxCM) obtained from carbonized coconut endocarp, and subsequently loaded with titanium-containing particles to produce CF/TClVS-OxCM-TiO_2. The materials were characterized by ATR-FTIR, solid-state UV–Vis spectroscopy, thermogravimetric analysis, SEM, and EDS. OxCM exhibited oxygen-containing functionalities and lower thermal stability than the original carbon, while remaining distinguishable from graphite-derived graphene oxide. The final composite showed increased surface roughness, detectable Si and Ti signals, and a decrease in the C/O mass ratio from 2.23 ± 0.44 to 0.77 ± 0.33. Under dark conditions, apparent PQT removal reached 32.81 ± 2.64% after 6 h and 47.27 ± 2.85% after 72 h. Direct solar exposure without material produced approximately 7.8% removal after 6 h, whereas the irradiated hybrid system yielded an apparent residual PQT concentration of 3.43 ± 0.06 ppm. After correction for the irradiated control, material-associated removal was approximately 58.5%, with an operationally estimated additional irradiation-associated contribution of 25.7 percentage points relative to dark adsorption. These findings demonstrate the feasibility of integrating complementary coconut biomass fractions into a multifunctional hybrid material and provide preliminary evidence of enhanced apparent PQT removal under natural sunlight.

Keywords: coconut biofibers; oxidized carbonaceous material; titanium dioxide; paraquat; photocatalysis; adsorption

Check for updates

Academic Editor: Andrea Petrella

Received: 21 September 2026
Revised: 14 October 2026
Accepted: 21 October 2026
Published: 22 October 2026

Copyright: © 2026 by the authors. Licensee MDPI, Basel, Switzerland. This article is an open access article distributed under the terms and conditions of the Creative Commons Attribution (CC BY) license.

1. Introduction

The increasing occurrence of agrochemicals in aquatic environments has stimulated the development of treatment technologies capable of removing highly soluble and biologically hazardous organic contaminants from water. Paraquat (PQT; 1,1′-dimethyl-4,4′-bipyridinium dichloride) is a highly polar cationic herbicide that has been extensively used because of its effectiveness and relatively low cost. Nevertheless, its release into soil and water represents an environmental concern because of its toxicity toward biological systems and its potential occurrence in aqueous environments [1,2]. Accordingly, several

approaches have been investigated for PQT removal, including adsorption, electrochemical processes, membrane separation, biological treatments, and advanced oxidation processes. Among these alternatives, adsorption onto carbonaceous materials is particularly attractive because PQT interacts effectively with oxygen-containing and aromatic surfaces; however, adsorption transfers the contaminant from the aqueous phase to a solid phase rather than destroying the parent molecule [2,3].

Heterogeneous photocatalysis offers a complementary strategy because absorbed photons with sufficient energy can generate electron–hole pairs in a semiconductor. The photogenerated charge carriers can subsequently participate in reduction and oxidation processes leading to reactive oxygen species and, ultimately, transformation of adsorbed or dissolved organic molecules. Titanium dioxide (TiO_2) remains one of the most extensively investigated photocatalysts because of its chemical stability, relatively low toxicity, availability, and photocatalytic activity. However, conventional TiO_2 exhibits important limitations for solar applications, particularly its weak response to the visible fraction of sunlight and rapid recombination of photogenerated charge carriers [4]. For PQT specifically, TiO_2-based photocatalytic systems have demonstrated substantially greater degradation than direct photolysis, confirming the suitability of this semiconductor for transformation of the bipyridinium herbicide [5]. Nevertheless, photocatalytic disappearance of the parent compound should not automatically be interpreted as complete mineralization because intermediate transformation products may also be generated during irradiation.

One strategy for improving TiO_2-based photocatalytic systems is its combination with carbonaceous materials. Graphene oxide and related oxidized carbon structures provide oxygen-containing surface groups and aromatic domains that can enhance pollutant adsorption while also promoting interfacial interactions with TiO_2. Carbonaceous phases may additionally act as electron acceptors or charge-transfer media, thereby reducing electron–hole recombination under appropriate interfacial conditions. Nguyen-Phan et al. [6] demonstrated that combining TiO_2 with graphene oxide enhanced both adsorption and photocatalytic removal relative to TiO_2 alone, illustrating the concept of adsorption-enhanced photocatalysis. More generally, TiO_2/graphene-based materials have been extensively investigated because the carbonaceous phase can contribute adsorption sites, interfacial charge transport, and improved utilization of the incident radiation [4]. Importantly for a biomass-valorization approach, oxidized carbonaceous materials and graphene-like structures can also be obtained from renewable carbon precursors. Coconut-shell-derived oxidized carbon has already been combined with TiO_2 for photocatalytic applications, demonstrating the feasibility of using coconut endocarp as a carbon source rather than relying exclusively on graphite-derived materials [7]. These studies demonstrate the potential of TiO_2/carbonaceous composites for adsorption-assisted photocatalytic applications, including systems incorporating coconut-derived carbon. However, they do not address the particular integration of coconut mesocarp-derived fibers and endocarp-derived oxidized carbon within the same silane-modified support for exploring solar-assisted PQT removal.

A second challenge is the configuration of photocatalytic material. The use of free fine particles can complicate solid recovery after treatment, whereas immobilization on a macroscopic support facilitates material manipulation and provides an opportunity to construct multifunctional interfaces. Cellulosic fibers are particularly attractive in this context because their hydroxyl-rich surfaces can be chemically modified and subsequently used for deposition of inorganic particles. Layer-by-layer immobilization of TiO_2 on surface-modified cellulose fibers has previously been demonstrated, showing that lignocellulosic substrates can serve as supports for TiO_2-based functional materials [8]. Organosilanes are especially useful as interfacial coupling agents because they can react with or condense on

hydroxyl-rich cellulose surfaces, producing Si–O–C and Si–O–Si-containing interphases that provide additional functionality for subsequent material deposition [9].

On the other hand, coconut-derived biomass provides a particularly interesting platform for this concept because different anatomical fractions of the same agricultural residue can fulfill complementary functions. Aged coir fibers obtained from the coconut mesocarp are hollow, micrometric lignocellulosic structures with chemically modifiable surfaces and have previously been proposed as support for the fabrication of functional polymeric materials [10]. In parallel, the carbon-rich endocarp can be carbonized and oxidized to generate an oxygen-functionalized carbonaceous material. Thus, instead of using the fibrous and carbon-rich fractions independently, an integrated design can exploit the coir fiber as a macroscopic support and the oxidized endocarp-derived carbon as an adsorptive/interfacial component. This approach also avoids assuming that biomass oxidation necessarily produces conventional graphite-derived graphene oxide; accordingly, the carbon phase investigated here is conservatively designated as oxidized carbonaceous material (OxCM).

Although TiO_2-based photocatalysis for PQT transformation [5], TiO_2/graphene oxide composites [6], coconut-derived carbon/TiO_2 materials [7], and surface-modified cellulosic supports [8–10] have been previously investigated, their integration into a single hybrid architecture remains comparatively underexplored. In particular, the sequential modification of mesocarp-derived coir fibers with TClVS, followed by incorporation of oxidized carbonaceous material from coconut endocarp and a titanium-containing phase, provides an opportunity to exploit complementary functions of distinct coconut biomass fractions. Accordingly, this study aimed to prepare and physicochemically characterize CF/TClVS-OxCM-TiO_2 and conduct a preliminary evaluation of its performance toward PQT removal under dark and direct natural solar-irradiation conditions.

2. Materials and Methods

2.1. Reagents

The coconuts used to obtain coconut fibers and endocarp-derived carbonaceous material were purchased from a local market. Titanium isopropoxide (97%), absolute ethanol, trichlorovinylsilane (TClVS, 97%), dimethyl sulfoxide (DMSO), $NaNO_3$, H_2SO_4 (95–97%), $KMnO_4$, and NaOH were purchased from Merck KGaA (Darmstadt, Germany). H_2O_2 (50%) was supplied by Agenquímicos (Cali, Colombia). A commercial PQT (200 g L^{-1}, Gramoxone® SL) was obtained from Syngenta S.A. (Bogotá, Colombia).

2.2. Preparation of TiO_2 Particles

TiO_2 particles were prepared by the dropwise addition of 12.0 mL of titanium isopropoxide to 250 mL of ethanol under continuous stirring. After completion of the addition, the resulting mixture was then stored at approximately 4 °C until use. Details of the physicochemical characterization of the obtained particles are provided in Section 2.7.

2.3. Preparation of Coconut Fibers

Coconut biofibers were obtained following the procedure reported by Palencia et al. [10]. Mature coconuts purchased from a local market were used as raw material. The fibers were obtained from the fruit mesocarp and had undergone prolonged exposure to environmental conditions before processing; therefore, they were referred to as aged coir fibers. During washing, the fibers released water-soluble substances that imparted a brown coloration to the aqueous medium. Consequently, the fibers were mechanically rubbed and repeatedly washed with water until no visible coloration was observed in the washing medium. The

washed fibers were then dried at 105 °C for 24 h. The physicochemical and morphological characteristics of aged coir fibers have been described previously [10] (see Figure 1).

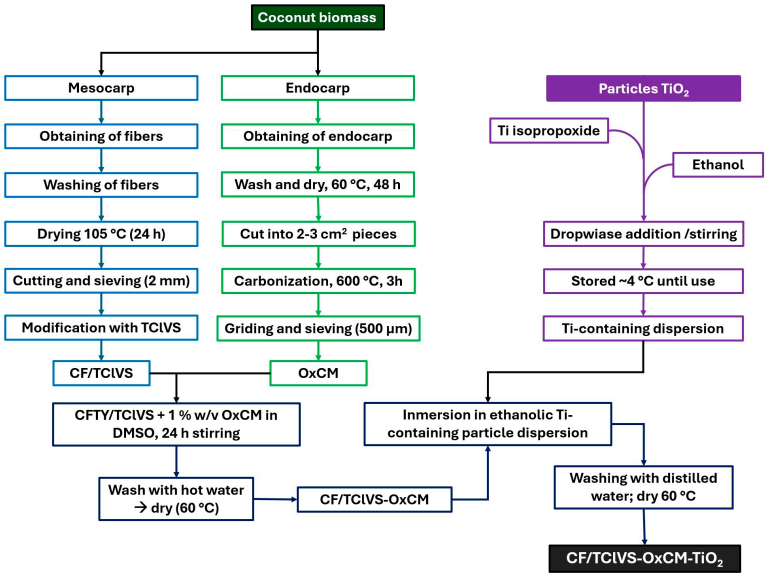


Figure 1. Schematic representation of the preparation of CF/TClVS-OxCM-TiO_2 through sequential modification of coconut mesocarp-derived fibers, incorporation of endocarp-derived oxidized carbonaceous material, and addition of titanium-containing particles.

2.4. Preparation of Oxidized Carbonaceous Material (OxCM)

To prepare OxCM, coconut endocarp was washed with distilled water and dried at 60 °C for 48 h. The dried material was cut into approximately 2–3 cm^2 pieces and carbonized in a muffle furnace at 600 °C for 3 h. The resulting carbon was ground using a NutriBullet NB-201 and sieved through a 500 µm mesh. The carbon was subsequently oxidized using the Hummers method, as described by Sujiono et al. [11]. Briefly, 14 g of carbon was mixed with 7.0 g of $NaNO_3$ and 175 mL of concentrated H_2SO_4 and stirred in an ice bath for 30 min. Subsequently, 42 g of $KMnO_4$ was slowly added, and the mixture was stirred continuously for 3 h. The ice bath was then removed, and stirring was continued for an additional 1 h, followed by the slow addition of 2 L of distilled water. Finally, 70 mL of a commercial 50% H_2O_2 solution was slowly added to terminate the oxidation reaction. The resulting material was filtered and washed repeatedly until neutral pH was achieved, using 0.4 M NaOH when required. The final OxCM was dried at 60 °C for 24 h.

For comparison, OxCM was evaluated alongside graphite-derived graphene oxide (GO) prepared using the Hummers method. The previously characterized GO was kindly provided by Prof. Hernán Valle from the Department of Chemistry, Universidad de Córdoba (Montería, Colombia). The characterization methods are described in Section 2.7, and the preparation scheme is illustrated in Figure 1.

2.5. Preparation of Coconut Fibers Doped with OxCM and TiO_2 Particles

To prepare the hybrid material, coconut fibers were cut using a guillotine-type cutter and sieved through a 2 mm mesh. The resulting fibers were placed in the outer compartment of a vessel consisting of two concentric cylinders, while TClVS (1.0 mL per gram of fiber) was added to the inner cylinder. Upon heating, TClVS vaporized and diffused throughout the sealed vessel. Given the hollow structure and pronounced surface roughness of the fibers, TClVS vapor was expected to reach both their external surfaces and internal cavities, potentially promoting modification of both regions. The vessel was hermetically sealed and maintained at 60 °C for 24 h.

After this treatment, the TClVS-modified fibers were immersed in a 1% (*w*/*v*) dispersion of OxCM in DMSO and maintained under continuous agitation for 24 h. The fibers were subsequently washed repeatedly with hot water to remove loosely bound OxCM and residual DMSO, followed by drying at 60 °C for 24 h.

To incorporate TiO_2 particles, the OxCM-containing fibers were immersed in the previously prepared ethanolic TiO_2 dispersion and stirred at room temperature for 24 h. The fibers were then recovered, washed with distilled water, and dried at 60 °C. The resulting hybrid material was designated CF/TClVS-OxCM-TiO_2. The preparation procedure is illustrated in Figure 1, and the characterization methods are described in Section 2.7.

2.6. Evaluation of PQT Photocatalytic Degradation by CF/TClVS-OxCM-TiO_2

For the solar-irradiation experiments, 5.0 mL of an aqueous PQT solution (10.19 ppm, pH 7.0) was mixed with 10 mg of CF/TClVS-OxCM-TiO_2. The mixture was gently stirred for 5 min and then exposed to direct sunlight for 6 h at ambient temperature, without active temperature control. Solar irradiance was not measured. A control solution containing PQT without the hybrid material was subjected to the same initial stirring and irradiation conditions. These experiments were intended to provide a preliminary assessment of material-assisted PQT removal under natural sunlight rather than to determine irradiation-dependent kinetic parameters or optimize photocatalytic operating conditions.

To assess the contribution of adsorption to apparent PQT removal, 5.0 mL of the same PQT solution was mixed with 10 mg of CF/TClVS-OxCM-TiO_2 and gently stirred for 5 min. The experimental vessels were then wrapped in aluminum foil and kept in the shade to prevent light exposure. Residual PQT concentrations were determined after 6, 24, 48, and 72 h. Both dark and solar-irradiation experiments were performed in duplicate. The selected initial PQT concentration (10.19 mg L^{-1}) and composite dosage (2.0 g L^{-1}) were fixed experimental conditions and were not optimized. The experiments were conducted using a fixed adsorbent dosage of 2.0 g L^{-1} (10 mg of composite in 5.0 mL of solution) and an initial PQT concentration of approximately 10.19 mg L^{-1}. These conditions were used for the preliminary evaluation of the hybrid material under dark and solar-irradiation conditions. The selected values represent experimental working conditions rather than optimized adsorbent dosage or pollutant concentration.

PQT concentrations were determined using a V-750 UV–Vis spectrophotometer (JASCO Corp., Tokyo, Japan) by measuring absorbance at 257 nm. Calibration was performed using PQT standards ranging from 2.0 to 7.0 ppm at pH 7.0. The calibration relationship was expressed as $A = aC + b$, where A and C represent absorbance and PQT concentration, respectively. The resulting calibration parameters were $a = 0.1053$ ppm^{-1}, $b = -0.0021$, and $R^2 = 0.9983$.

2.7. Characterization Analyses

ATR-FTIR spectra were acquired using an IRAffinity-1S Fourier-transform infrared spectrophotometer (Shimadzu Corp., Kyoto, Japan) equipped with an attenuated total reflectance (ATR) accessory containing a ZnSe crystal. Spectra were recorded over the range of 4000–600 cm^{-1} using 30 scans at a resolution of 2 cm^{-1}. Solid-state UV–Vis spectra were obtained using a V-750 UV–Vis spectrophotometer equipped with an SV-922 integrating sphere (JASCO Corp., Tokyo, Japan), at a spectral resolution of 0.5 nm over the range of 200–800 nm. Because PQT concentrations were determined from UV–Vis absorbance at 257 nm, the corresponding concentration decreases were interpreted as apparent PQT removal. This analytical approach does not independently distinguish adsorption from chemical transformation under irradiation or establish mineralization and the identity of transformation products.

Dynamic light scattering (DLS, Malvern Panalytical, Malvern, UK) was used to determine the hydrodynamic radius of TiO_2 particles in aqueous dispersion. Measurements were performed in duplicate.

Thermogravimetric analyses (TGA) of coconut endocarp-derived carbon, OxCM, and GO were performed using a Q50 thermogravimetric analyzer (TA Instruments, New Castle, DE, USA) under a nitrogen atmosphere. Samples were heated from 25 to 900 °C at a heating rate of 10 °C min^{-1}.

Scanning electron microscopy (SEM) analyses were performed using a Phenom ProX microscope (Thermo Fisher Scientific, Waltham, MA, USA). Prior to examination, the samples were coated with a thin layer of gold. Energy-dispersive X-ray spectroscopy (EDS) was additionally employed for local elemental characterization of representative regions of the materials.

3. Results and Discussion

3.1. Preparation and General Characterization of TiO_2 Particles

Characterization of the product obtained from titanium isopropoxide provided complementary evidence consistent with the formation of a titanium oxide-containing particulate phase. DLS revealed an intensity-weighted hydrodynamic diameter distribution extending from approximately 108 to 198 nm, with the highest contribution centered at about 146 nm (Figure 2A). The UV–Vis spectrum exhibited pronounced absorption in the UV region, with a maximum at approximately 308 nm and substantially lower absorbance in the visible region, consistent with the optical behavior of titanium oxide-based materials (Figure 2B). In addition, five replicate ATR-FTIR measurements showed reproducible spectral features, including a broad O–H contribution around 3200–3300 cm^{-1}, bands associated with residual organic groups from the precursor, and a pronounced absorption near 668 cm^{-1}, consistent with Ti–O vibrations (Figure 2C,D). Together, these observations support the formation of a particulate phase containing Ti–O environments, although they do not establish its precise chemical or crystalline phase composition. Nevertheless, the present characterization was not intended to resolve the crystalline structure or distinguish among possible TiO_2 polymorphs; therefore, a more detailed analysis of crystallinity, phase composition, and particle nanostructure should be considered in future studies using complementary techniques such as X-ray diffraction and high-resolution electron microscopy.

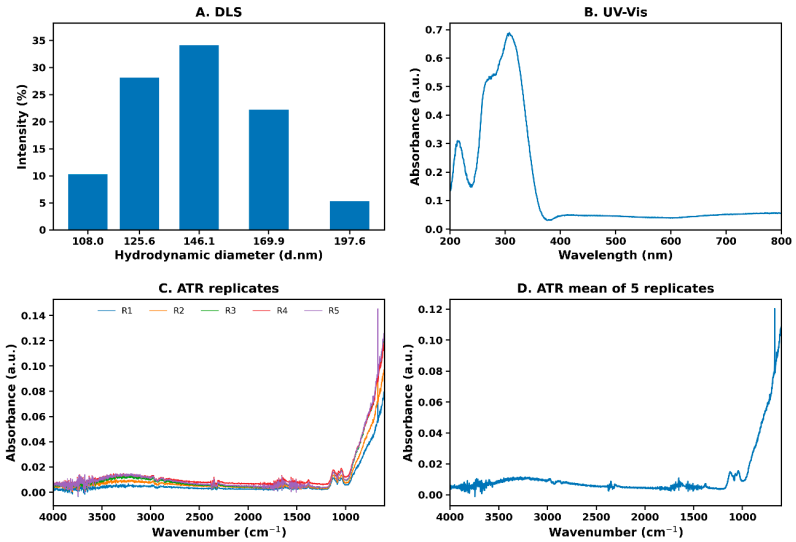


Figure 2. Characterization of TiO_2 particles: (**A**) particle size distribution obtained by DLS; (**B**) solid-state UV–Vis spectrum; (**C**) ATR-FTIR spectra of five independent replicates (R1–R5); and (**D**) mean ATR-FTIR spectrum of the five replicates.

The preparation of the titanium-containing phase was based on a simplified solution-processing procedure without a separate calcination or purification step. This approach was intended to minimize the number of preparation operations while providing a titanium-containing component for incorporation into the hybrid material. The combined DLS, UV–Vis, and ATR-FTIR results are consistent with the formation of a particulate phase containing Ti–O environments. However, the available characterization does not establish its precise phase composition or crystalline structure. Since the present study focused on the preliminary functional evaluation of the integrated composite rather than on establishing relationships between TiO_2 polymorphism and photocatalytic activity, detailed crystallographic characterization was beyond its experimental scope. Future XRD analyses would be valuable for investigating these relationships and guiding subsequent optimization of the material.

3.2. TClVS-Modified Coconut Fibers

The changes in the visual appearance of coconut fibers during processing are shown in Figure 3A–C. Untreated aged fibers (Figure 3A) exhibit the heterogeneous brown appearance characteristic of natural coir, whereas washed fibers (Figure 3B) display a more uniform light-brown/orange coloration. Following TClVS treatment, the fibers become markedly darker (Figure 3C), providing an initial macroscopic indication of surface modification.

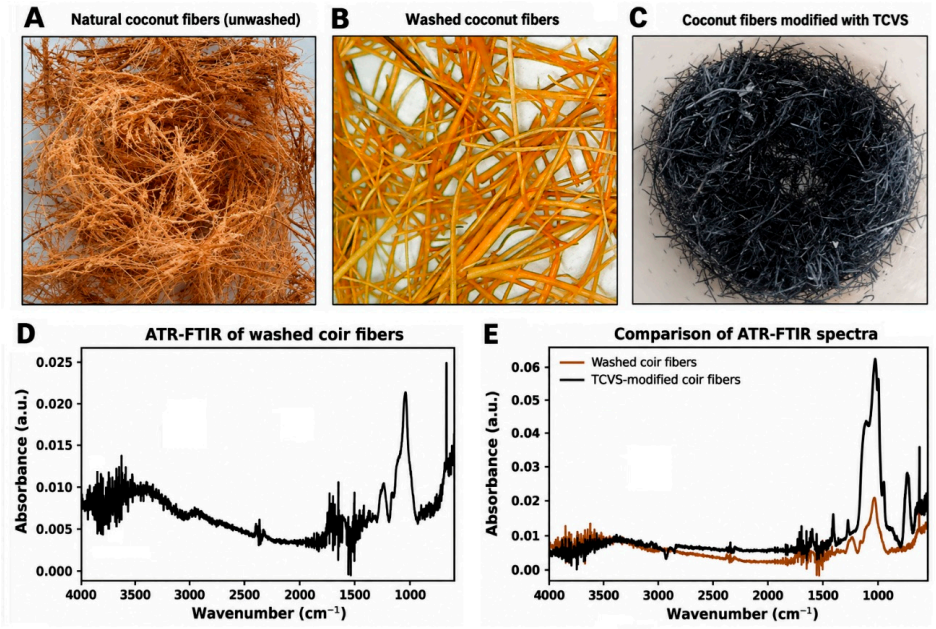


Figure 3. Images showing the visual appearance of natural, washed, and TClVS-modified coconut fibers (**A**, **B**, and **C**, respectively); (**D**) ATR-FTIR spectrum of washed coconut fibers; and (**E**) comparison of the ATR-FTIR spectra of washed and TClVS-modified coconut fibers.

The ATR-FTIR spectrum of washed coir fibers (Figure 3D) exhibits the characteristic features of lignocellulosic materials. The broad band between approximately 3600 and 3200 cm^{-1} is associated with O–H stretching vibrations of hydrogen-bonded hydroxyl groups in cellulose, hemicellulose, and lignin, while the band near 2940 cm^{-1} is primarily attributed to aliphatic C–H stretching of methyl and methylene groups. A weak feature at approximately 1725–1730 cm^{-1} is consistent with C=O stretching of acetyl and uronic ester groups in hemicellulose and nonconjugated carbonyl-containing structures in lignin. The band near 1605 cm^{-1} is associated mainly with aromatic skeletal vibrations of lignin, potentially overlapping with contributions from adsorbed water, while additional lignin-related aromatic vibrations occur near 1510 cm^{-1}. The absorption between 1240 and 1250 cm^{-1} is

primarily associated with C–O vibrations of lignin and hemicellulose. Finally, the intense band near 1040 cm^{-1} arises mainly from C–O and C–O–C stretching vibrations within the polysaccharide framework, particularly cellulose. Overall, these spectral features are consistent with the cellulose–hemicellulose–lignin composition expected for coir fibers [10,12].

TClVS treatment produces noticeable changes in the ATR-FTIR spectrum (Figure 3E). Although the principal lignocellulosic bands remain detectable, the modified fibers exhibit increased absorbance between 1000 and 1100 cm^{-1}, a more pronounced contribution near 760–780 cm^{-1}, and changes around 1600 cm^{-1}. These variations are consistent with the formation of silicon-containing surface species. In organosilane-modified cellulose, Si–O–C and Si–O–Si stretching vibrations generally contribute to the 1000–1150 cm^{-1} region, although their individual assignments are complicated by overlap with the intense C–O and C–O–C absorptions of cellulose [13]. Furthermore, vinyl-functionalized cellulose has been reported to exhibit C=C stretching near 1604 cm^{-1} and Si–O/Si–C-associated contributions around 760 cm^{-1} [14]. Accordingly, the combined spectral changes support the incorporation of vinyl-containing silicon species onto the lignocellulosic surface, although individual bands cannot be assigned unambiguously to specific interfacial bonds.

The expected reactivity of TClVS provides a plausible chemical explanation for these observations. Trichlorosilanes readily react with hydroxylated surfaces, and gas–solid modification of cellulose with related compounds has been shown to generate Si–O–Si networks partially attached to polysaccharide chains through Si–O–C linkages [9]. In the present system, surface hydroxyl groups from cellulose and lignin may react with the electrophilic silicon center of TClVS through substitution of Si–Cl groups, forming surface Si–O bonds with the release of HCl. Simultaneously, residual or adsorbed water within the lignocellulosic matrix may hydrolyze Si–Cl groups to form silanols, which can subsequently condense with fiber hydroxyl groups or undergo self-condensation to produce Si–O–Si-containing oligomeric domains. Thus, direct surface coupling and hydrolysis–condensation reactions may occur concurrently rather than representing mutually exclusive pathways. This interpretation is consistent with previous studies describing fiber–silane coupling and siloxane-network formation during cellulose modification [9,13,15].

Nevertheless, the ATR-FTIR results should be interpreted as evidence consistent with TClVS incorporation rather than definitive proof of a single, structurally uniform surface species. Because Si–O–C and Si–O–Si vibrations overlap with the native C–O absorptions of cellulose, multiple silicon-containing environments may contribute to the observed spectral changes. Such chemical heterogeneity is consistent with the coexistence of cellulose and lignin hydroxyl groups, residual moisture, and neighboring silane molecules that may participate in the modification process [16].

3.3. Preparation and Characterization of the Oxidized Carbonaceous Material (OxCM)

The chemical changes induced by oxidation of coconut endocarp-derived carbon were initially examined by ATR-FTIR spectroscopy, using the unoxidized carbon and graphite-derived graphene oxide (GO), prepared through a Hummers-type method, as reference materials (Figure 4A). The carbon precursor exhibits relatively weak and broad spectral features, as expected for a highly carbonized material. These include contributions near 1600 cm^{-1} attributable to aromatic C=C vibrations and/or adsorbed water, a band at approximately 1350–1400 cm^{-1} associated with C–H deformation, and absorptions below 1200 cm^{-1} related to residual C–O functionalities. Following oxidation, the OxCM spectrum shows more pronounced features associated with oxygen-containing groups, including a carbonyl-related band near 1700 cm^{-1}, contributions from aromatic C=C domains at approximately 1550–1600 cm^{-1}, and additional absorptions within the 1300–900 cm^{-1} fingerprint region. The latter may arise from C–O-containing functionalities,

including alcohol, phenolic, and epoxide groups. Similar oxygen-containing functionalities have been reported in coconut-shell-derived materials oxidized using the Hummers method [11]. Nevertheless, these assignments should be interpreted cautiously because several vibrational modes overlap extensively in oxidized carbonaceous materials [17].

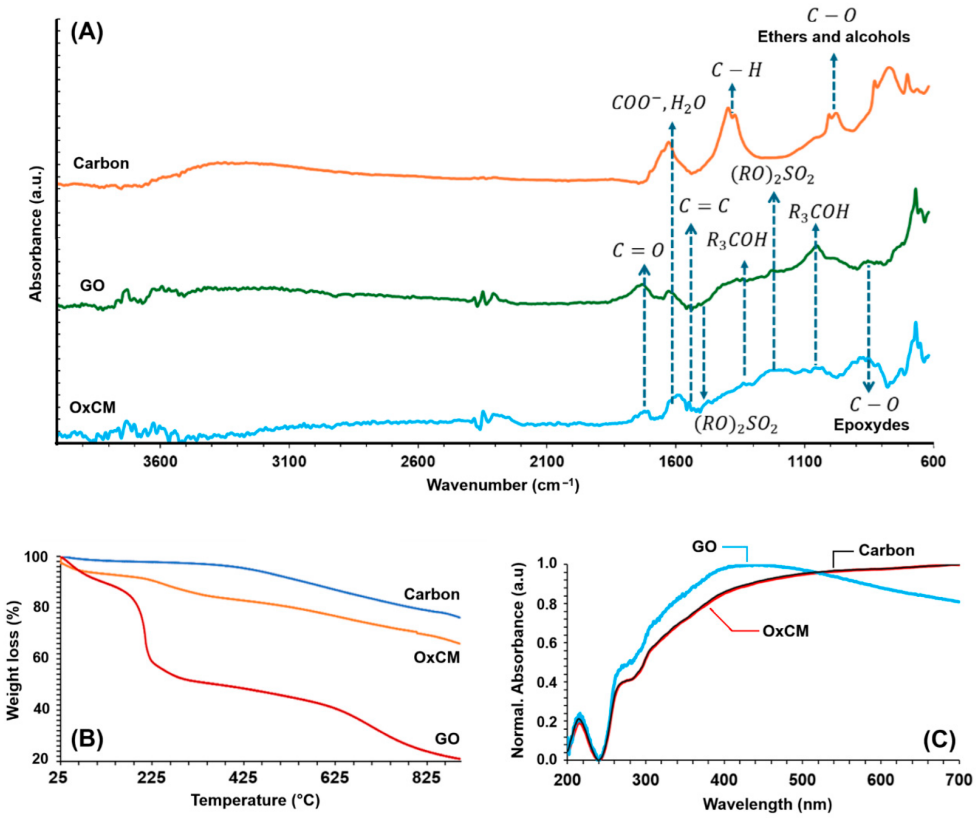


Figure 4. Physicochemical characterization of carbonaceous materials. (**A**) ATR-FTIR spectra, (**B**) thermogravimetric profiles, and (**C**) solid-state UV–Vis spectra of coconut endocarp-derived carbon (Carbon), oxidized carbonaceous material (OxCM), and graphite-derived graphene oxide (GO).

Compared with OxCM, graphite-derived GO exhibits more clearly resolved spectral features associated with oxygen-containing functionalities, including carbonyl and C–O groups, as well as contributions attributable to tertiary alcohol and epoxide environments. Additional bands may arise from sulfate-containing species introduced during Hummers oxidation. Previous studies have demonstrated that covalently bound organosulfate species can persist in Hummers-derived GO even after extensive aqueous washing, with absorptions overlapping those of C–O functionalities in the fingerprint region [17,18]. Although OxCM exhibits analogous spectral features, they are less clearly resolved than those of graphite-derived GO. These differences are consistent with oxidation and surface functionalization of coconut-derived carbon without the formation of a material spectroscopically identical to conventional graphite-derived GO. Such differences are expected because the coconut-derived precursor is structurally more heterogeneous than graphite and may develop a different distribution of oxygen-containing functionalities upon oxidation.

Thermogravimetric analysis provides complementary evidence of these differences (Figure 4B). The unoxidized carbon exhibits the highest thermal stability, retaining approximately 75% of its initial mass at the upper end of the investigated temperature range. In contrast, graphite-derived GO undergoes pronounced mass loss at approximately 200–250 °C, followed by further decomposition at higher temperatures, ultimately retaining about 20% of its initial mass. This behavior is characteristic of oxidized graphenic materials, in which

physically adsorbed water is released at relatively low temperatures, while thermally labile oxygen-containing groups decompose predominantly between approximately 150 and 300 °C, releasing volatile products such as H_2O, CO, and CO_2 [19]. Hummers-derived materials may also undergo mass loss associated with the decomposition of organosulfate species within approximately 200–300 °C [18].

OxCM exhibits an intermediate thermal response, with greater mass loss than the original carbon but substantially less than graphite-derived GO. Unlike GO, OxCM does not display an equally pronounced decomposition step, instead undergoing a more gradual mass loss throughout the investigated temperature range. This behavior is consistent with the introduction of thermally labile oxygen-containing functionalities while retaining a substantial fraction of the original carbonaceous framework. Similar variations in thermal stability have been associated with differences in the abundance and stability of surface oxygen groups in oxidized carbon materials [19]. Thus, the TGA results support the ATR-FTIR observations and further distinguish OxCM from both the unoxidized precursor and graphite-derived GO.

Solid-state UV–Vis spectroscopy provides additional information on the optical properties of these materials (Figure 4C). All three samples exhibit absorption in the UV region, including a high-energy feature near 210–220 nm and spectral contributions extending approximately from 270 to 310 nm. In oxidized graphenic materials, absorption near 230 nm is commonly attributed to $\pi \rightarrow \pi^*$ transitions of aromatic sp^2 domains, whereas weaker absorption around 300 nm is generally associated with $n \rightarrow \pi^*$ transitions involving carbonyl-containing groups [20]. Comparable optical features have been reported for graphene-like materials prepared from coconut-shell carbon using modified Hummers oxidation [11].

The OxCM spectrum retains similarities to that of the original carbon while exhibiting changes in the UV region consistent with modifications of the electronic environment following oxidation. In contrast, graphite-derived GO displays a broader optical response and a distinct spectral profile, reflecting differences in the carbonaceous framework and oxidation-related functionalities. Because the spectra in Figure 4C are presented as normalized absorbance, differences in signal intensity should not be used to quantify the relative abundance of oxygen-containing groups. Instead, comparisons should focus on spectral shape, band positions, and changes in the observed absorption features.

Overall, the complementary ATR-FTIR, TGA, and UV–Vis results support the incorporation of oxygen-containing functionalities into coconut endocarp-derived carbon while indicating retention of a substantial fraction of its original carbonaceous structure. Accordingly, the designation oxidized carbonaceous material (OxCM) is more appropriate than graphene oxide for the product obtained, with graphite-derived GO serving as a reference for evaluating the effects of oxidation.

3.4. Preparation of TClVS-Modified Coconut Fibers Impregnated with OxCM and TiO_2 Particles

The sequential modification of coconut fibers was evaluated by ATR-FTIR spectroscopy (Figure 5a–d). The spectrum of washed fibers (Figure 5a) exhibits the characteristic features of a lignocellulosic substrate, including carbonyl-related contributions at approximately 1700–1750 cm^{-1}, aromatic C=C vibrations associated mainly with lignin near 1600 cm^{-1}, and intense C–O/C–O–C absorptions below 1250 cm^{-1}. Following TClVS treatment (Figure 5b), pronounced spectral changes appear within the 1150–950 and 800–700 cm^{-1} regions. These changes are consistent with the incorporation of silicon-containing species, although the overlap between cellulose vibrations and Si–O–C, Si–O–Si, and Si–C-associated contributions prevents unambiguous assignment of individual interfacial bonds. Similar spectral changes have been reported for cellulose modified with volatile trichlorosilanes,

where siloxane networks partially attached to the polysaccharide chains were formed [9]. Furthermore, vinyltrichlorosilane can undergo hydrolysis and condensation to produce polysiloxane-type coatings [21].

The solid byproduct generated during TClVS treatment (Figure 5e) provides additional information about these reactions. Its ATR-FTIR spectrum exhibits pronounced contributions within the 1100–950 and 750–800 cm^{-1} regions, resembling those observed for the TClVS-modified fibers. This spectral similarity is consistent with hydrolysis and self-condensation of TClVS occurring alongside fiber functionalization. Therefore, the modification process may involve both reactions between Si–Cl groups and accessible hydroxyl groups of the lignocellulosic substrate and the formation of oligomeric or polymeric Si–O–Si domains. These pathways are consistent with the known reactivity of trichlorosilanes toward hydroxylated surfaces and moisture [9].

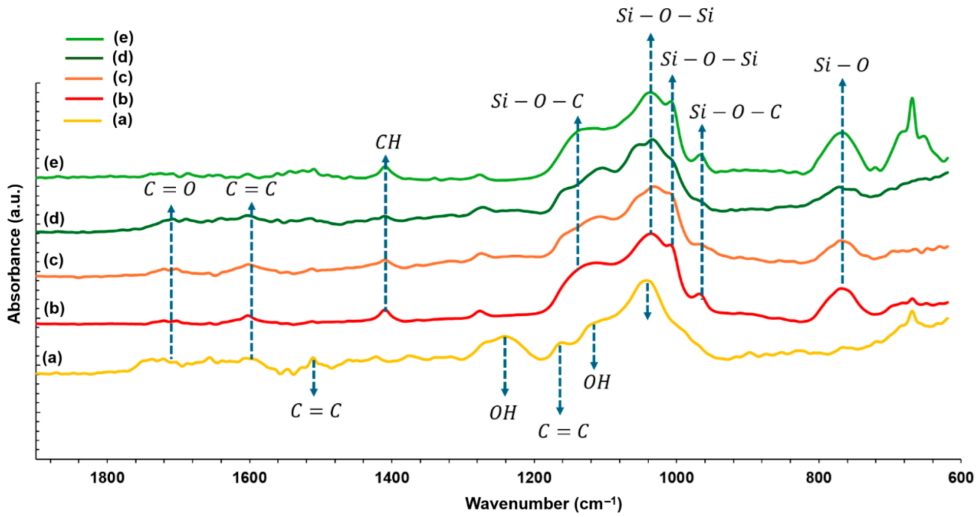


Figure 5. ATR-FTIR spectra of coconut fibers at successive stages of modification: (a) washed coconut fibers (CFs), (b) TClVS-modified fibers (CF/TClVS), (c) fibers loaded with oxidized carbonaceous material (CF/TClVS-OxCM), (d) fibers subsequently loaded with titanium-containing particles (CF/TClVS-OxCM-TiO_2), and (e) solid byproduct obtained during TClVS treatment.

Subsequent incorporation of OxCM produces additional spectral changes (Figure 5c). Compared with the TClVS-modified fibers, the CF/TClVS-OxCM material exhibits more pronounced contributions within the carbonyl/aromatic region at approximately 1700–1550 cm^{-1}, together with modifications in the 1300–900 cm^{-1} fingerprint region. These variations are consistent with the oxygen-containing functionalities and aromatic carbon domains previously identified in OxCM (Figure 4). However, the extensive overlap between these contributions and those of the lignocellulosic substrate and siloxane-containing interphase prevents unequivocal identification of OxCM from ATR-FTIR alone. Similar limitations have been reported for silane-crosslinked cellulose/graphene oxide systems, where incorporation of the carbonaceous phase was supported by complementary spectroscopic, morphological, and elemental evidence [22].

After the final loading step with titanium-containing particles (Figure 5d), the main spectral features of the CF/TClVS-OxCM material remain detectable, together with changes in the low-wavenumber region between approximately 800 and 600 cm^{-1}. TiO_2-containing cellulose materials commonly exhibit Ti–O-related absorptions below 800 cm^{-1}; however, these contributions overlap with cellulose skeletal vibrations and Si–O/Si–C-associated bands [23]. Consequently, the observed spectral changes are compatible with the incorporation of a titanium-containing phase but are not independently diagnostic of its

identity. The EDS results discussed below provide more direct elemental evidence of titanium incorporation.

SEM micrographs provide complementary evidence of the morphological changes induced by the modification process (Figure 6). Washed coconut fibers (Figure 6A,B) retain the characteristic hollow structure of coir, including a comparatively continuous external wall, longitudinal surface features, pores, and internal fibrillar structures. In contrast, the final CF/TClVS-OxCM-TiO_2 material (Figure 6D,E) exhibits a rougher and more heterogeneous surface, with layered and deposit-like structures covering or interspersed among the underlying lignocellulosic fibrils. Although these morphological changes cannot be attributed exclusively to OxCM or the titanium-containing phase, they are consistent with the deposition of additional components onto the fiber surface. Comparable morphological changes have been reported for silane-modified cellulose incorporating graphene oxide [22] and cellulose-supported TiO_2 composites prepared through sequential deposition procedures [8].

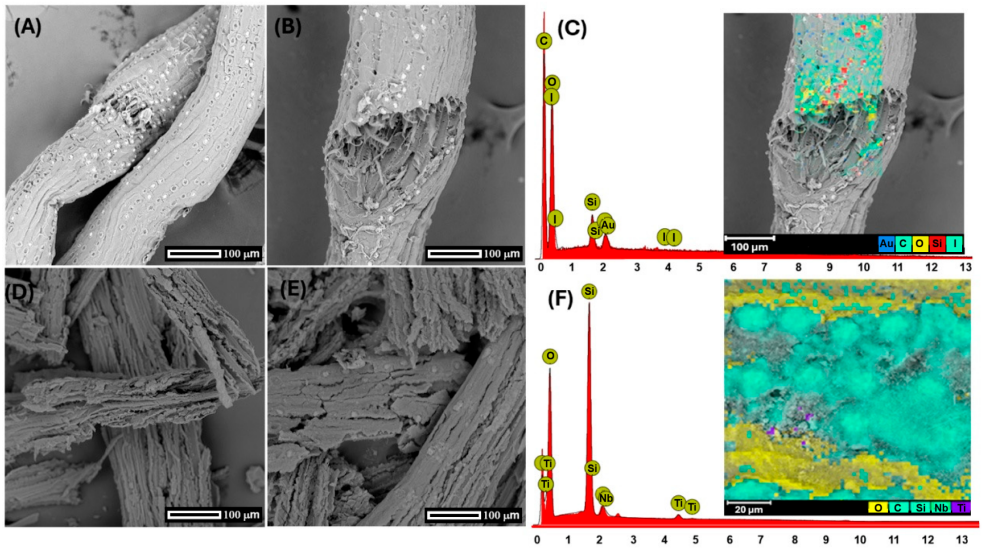


Figure 6. SEM and EDS characterization of washed coconut fibers and the final CF/TClVS-OxCM-TiO_2 composite: (**A**,**B**) SEM micrographs of washed fibers; (**C**) EDS spectrum and elemental distribution of washed fibers; (**D**,**E**) SEM micrographs of the final composite; and (**F**) EDS spectrum and elemental distribution of the final composite.

EDS provides further evidence of changes in the elemental composition of the fibers. The spectra of washed fibers (Figure 6C) are dominated by C and O, whereas the final composite (Figure 6F) exhibits a more pronounced Si contribution and clearly detectable Ti signals. The presence of Si is consistent with incorporation of the TClVS-derived interphase, while the Ti signals indicate that titanium-containing material remained associated with the fibers after the immersion and washing steps. Similar elemental evidence has been used to support TiO_2 deposition in cellulose-based photocatalytic composites [8,24].

The apparent Nb signal in Figure 6F requires particular consideration. None of the reagents used in the preparation provides an identified source of niobium, whereas a Au signal is present in the EDS spectrum of washed fibers (Figure 6C). The Nb Lα and Au Mα lines occur at approximately 2.166 and 2.120 keV, respectively, and their proximity can lead to incorrect assignments by automated EDS peak-identification algorithms. Newbury and Ritchie [25] identify this overlap as a recognized source of misidentification. Therefore, in the absence of independent evidence for niobium, the corresponding signal is more plausibly associated with Au originating from the conductive coating used for SEM/EDS analysis.

The EDS-derived C/O mass ratios provide additional, although nonspecific, evidence of changes in surface composition (Table 1). Washed fibers exhibit a mean C/O ratio of 2.23 ± 0.44, whereas the final composite has a substantially lower value of 0.77 ± 0.33, corresponding to a decrease of approximately 65%. Furthermore, all three C/O values measured for the final material (0.53–1.14) are lower than those obtained for washed fibers (1.72–2.52). These results indicate an increase in the relative oxygen contribution within the analyzed regions. Although this trend is consistent with OxCM incorporation, it cannot be attributed exclusively to this component because the TClVS-derived interphase and titanium-containing phase also contribute oxygen. Accordingly, the C/O decrease should be interpreted as evidence of overall oxygen enrichment rather than as a specific chemical marker of OxCM.

Table 1. Carbon-to-oxygen mass ratio (C/O) determined by EDS for washed coconut fibers (CFs) and TClVS-modified coconut fibers impregnated with OxCM and TiO_2 particles (CF/TClVS-OxCM-TiO_2).

Washed Coconut Fibers			**CF/TClVS-OxCM-TiO_2**		
C (%)	**O (%)**	**C/O**	**C (%)**	**O (%)**	**C/O**
20.61	11.98	1.72	14.88	12.99	1.14
70.94	29.06	2.44	24.60	46.58	0.53
71.61	28.39	2.52	11.53	17.80	0.64
Mean ± standard deviation		2.23 ± 0.44	Mean ± standard deviation		0.77 ± 0.33

Taken together, ATR-FTIR, SEM, and EDS provide complementary evidence supporting the sequential construction of the CF → CF/TClVS → CF/TClVS-OxCM → CF/TClVS-OxCM-TiO_2 architecture. The spectroscopic changes are consistent with incorporation of silicon-containing and oxidized carbonaceous components, while the morphological and elemental results support the deposition and retention of additional phases, including titanium-containing particles, on the lignocellulosic support. Comparable strategies involving surface-modified cellulose, carbonaceous materials, and TiO_2 have been reported previously [8,22].

3.5. Effect of CF/TClVS-OxCM-TiO_2 on an Aqueous PQT Solution at pH 7.0

The decrease in PQT concentration under dark conditions demonstrates that CF/TClVS-OxCM-TiO_2 possesses an appreciable intrinsic adsorption capacity toward the herbicide. The residual PQT concentration decreased from 10.1944 ppm to 6.85 ± 0.27 ppm after 6 h, corresponding to an adsorption of 32.81 ± 2.64% and an adsorbed amount of approximately 1.67 mg g^{-1}. Adsorption continued with increasing contact time, reaching 40.86 ± 2.79%, 44.50 ± 2.85%, and 47.27 ± 2.85% after 24, 48, and 72 h, respectively. The corresponding adsorption capacities were approximately 2.08, 2.27, and 2.41 mg g^{-1} (see Table 2). Approximately 69.5% of the amount adsorbed after 72 h was retained during the first 6 h, indicating a relatively rapid initial uptake followed by a progressively slower increase in PQT adsorption. This behavior suggests that the adsorption process evolves over different timescales, although the available data do not allow the underlying mass-transfer or adsorption mechanisms to be distinguished.

The observed adsorption behavior may be associated with the chemically heterogeneous nature of CF/TClVS-OxCM-TiO_2. In particular, oxygen-containing functional groups and aromatic carbon domains introduced through OxCM incorporation may contribute to interactions with the cationic PQT species. Paraquat adsorption on carbonaceous materials has previously been associated with combinations of pore filling, hydrogen bonding, electrostatic interactions, and interactions involving carbonaceous domains, depending on surface chemistry and operating conditions [3,26]. Paraquat adsorption has also been

demonstrated on graphene-oxide-containing hybrid adsorbents, confirming the affinity of oxygen-rich carbonaceous surfaces toward this cationic herbicide [27]. However, the relative contributions of these mechanisms cannot be established from the present experiments, particularly because the specific surface area and pore size distribution of the hybrid material were not determined.

Table 2. Time-dependent adsorption of PQT onto CF/TClVS-OxCM-TiO_2 under dark conditions. Experimental conditions: 5.0 mL of aqueous PQT solution (10.19 ppm, pH 7.0) and 10 mg of CF/TClVS-OxCM-TiO_2. The residual PQT concentration in solution and the observed adsorption percentage is reported as mean ± standard deviation (n = 2).

Time (h)	Residual Concentration (ppm)	Adsorption (%)
6	6.85 ± 0.27	32.81 ± 2.64
24	6.03 ± 0.28	40.86 ± 2.79
48	5.66 ± 0.29	44.50 ± 2.85
72	5.38 ± 0.29	47.27 ± 2.85

Although adsorption continued throughout the investigated period, the incremental increase became progressively smaller, from approximately 8.1 percentage points between 6 and 24 h to 3.6 and 2.8 percentage points during the subsequent 24 h intervals. Approximately 69.5% of the amount adsorbed after 72 h was already retained within the first 6 h, indicating a higher average uptake during this initial interval than during the subsequent experimental periods. However, because no intermediate measurements were performed within the first 6 h, the detailed evolution of the initial adsorption rate and the possible occurrence of distinct kinetic stages cannot be established from the available data. Consequently, a more detailed kinetic characterization, particularly during the first 6 h, would require additional measurements at shorter contact times. Therefore, the present results should be interpreted as a descriptive evaluation of the time-dependent adsorption behavior rather than a comprehensive kinetic analysis.

On the other hand, the UV–Vis spectral evolution provides additional evidence for distinguishing direct photolysis, adsorption, and photoinduced removal of PQT (Figure 7). The characteristic PQT absorption maximum at approximately 257 nm progressively decreased depending on the experimental condition. Direct exposure of the PQT solution to solar irradiation for 6 h decreased its concentration from 10.19 to 9.40 ppm, corresponding to approximately 7.8% loss in the absence of CF/TClVS-OxCM-TiO_2. This relatively small decrease indicates that PQT undergoes some direct photolysis under the experimental irradiation conditions, consistent with previous reports showing slow paraquat photolysis in the absence of TiO_2 [5,28].

In the presence of CF/TClVS-OxCM-TiO_2 under dark conditions, the absorbance at 257 nm decreased progressively with contact time, in agreement with the independently determined adsorption values (see Table 2). In contrast, exposure of the PQT/CF/TClVS-OxCM-TiO_2 system to solar irradiation for 6 h produced a substantially larger decrease in the PQT band, resulting in a residual concentration of 3.43 ± 0.06 ppm. Therefore, the spectral decrease observed under irradiation cannot be attributed exclusively to either direct photolysis or adsorption.

After accounting for the decrease observed in the irradiated PQT control, the material-associated apparent removal was approximately 58.5%. Comparison with the 32.81 ± 2.64% removal observed under dark conditions after 6 h yielded an additional irradiation-associated contribution of approximately 25.7 percentage points. However, this difference represents an operational estimate and should not be interpreted as a quantitative measure

of photocatalytic degradation, since adsorption and light-induced processes may occur simultaneously and influence one another.

The greater decrease in the characteristic PQT absorption band at 257 nm under solar irradiation indicates enhanced apparent removal in the presence of CF/TClVS-OxCM-TiO_2. This behavior is consistent with a possible contribution from photocatalytic transformation, as previously reported for TiO_2-based systems [5,28]. Nevertheless, the UV–Vis measurements do not independently establish chemical degradation or distinguish potential transformation products from the parent compound. Furthermore, mineralization cannot be inferred from these measurements. Confirmation of these processes would require complementary analytical techniques, such as total organic carbon determination and chromatographic analyses. Accordingly, the present results demonstrate irradiation-associated enhancement of apparent PQT removal rather than a directly quantified photocatalytic degradation efficiency.

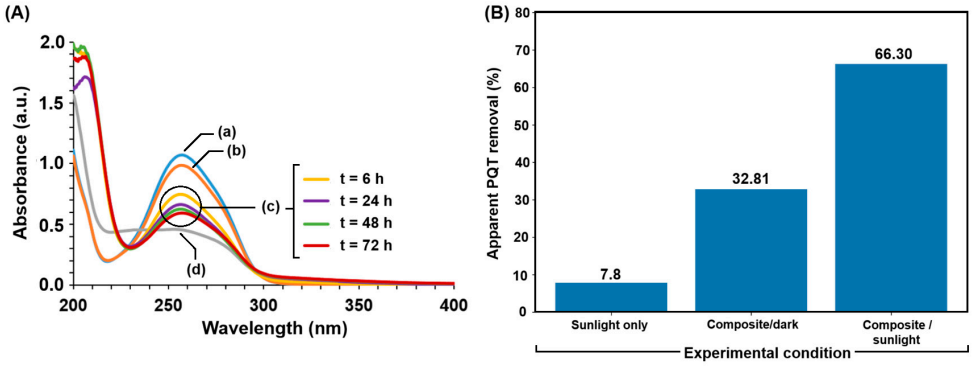


Figure 7. (**A**) UV–Vis spectral changes in PQT under different experimental conditions: (a) PQT solution maintained in the dark, (b) PQT solution exposed to direct solar irradiation, (c) PQT solution in contact with CF/TClVS-OxCM-TiO_2 under dark conditions for 6, 24, 48, and 72 h, and (d) PQT solution in contact with CF/TClVS-OxCM-TiO_2 and exposed to direct solar irradiation for 6 h. Experimental conditions: 5.0 mL of aqueous PQT solution (10.19 ppm, pH 7.0) and, where indicated, 10 mg of CF/TClVS-OxCM-TiO_2. (**B**) Comparison of apparent PQT removal after 6 h under direct solar irradiation without the hybrid material, dark adsorption using CF/TClVS-OxCM-TiO_2, and direct solar irradiation in the presence of CF/TClVS-OxCM-TiO_2. Experimental conditions: initial PQT concentration of approximately 10.19 mg L^{-1}, pH 7.0, solution volume of 5.0 mL, and composite dosage of 2.0 g L^{-1} when applicable. Apparent removal was estimated from UV–Vis measurements at 257 nm. The comparison does not establish the individual contributions of adsorption and photocatalytic degradation.

In addition, although the incorporation of Ti-containing particles into the hybrid material was supported by physicochemical characterization, the specific contribution of TiO_2 to the observed irradiation-associated enhancement cannot be independently established from the present experimental design. In particular, evaluating CF/TClVS-OxCM without TiO_2 under identical irradiation conditions would be necessary to distinguish the effect of TiO_2 incorporation from potential contributions of the carbonaceous phase and the lignocellulosic support. Therefore, the observed enhancement should be attributed to the integrated hybrid system rather than exclusively to the TiO_2 component.

The apparent PQT removal observed in the present study can be contextualized by comparison with previously reported adsorbents and photocatalytic systems. For example, Tongur and Ayranci [3] reported 47.1% PQT removal by adsorption onto activated carbon cloth, whereas Dehghani et al. [27] obtained a Langmuir maximum adsorption capacity of 31.34 mg g^{-1} using a graphene oxide/mesoporous silica composite under ultrasound-assisted conditions. In comparison, the present hybrid material exhibited 47.27 ± 2.85% adsorption after 72 h, corresponding to an experimentally determined up-

take of 2.41 mg g^{-1}. However, these values should not be interpreted as directly comparable performance indicators because of differences in experimental conditions and the distinction between measured uptake and model-derived maximum adsorption capacity. Regarding irradiation-assisted processes, Marien et al. [5] reported 91% total organic carbon removal using TiO_2/SiC under UV-C irradiation, while Moradi et al. [29] reported 80% PQT removal using a TiO_2/WO_3/diatomite composite under optimized simulated solar irradiation. These findings illustrate the performance of alternative material configurations while emphasizing that differences in irradiation conditions, analytical endpoints, and experimental design prevent direct quantitative ranking. Accordingly, the principal contribution of the present study lies in the preliminary evaluation of a coconut-biomass-derived hybrid architecture rather than in demonstrating superior removal efficiency relative to existing materials.

4. Conclusions and Remarks

In this study, a hybrid material was successfully prepared through the sequential modification of coconut coir fibers with TClVS, incorporation of oxidized carbonaceous material (OxCM) derived from coconut endocarp, and loading with titanium-containing particles. This strategy integrates two distinct fractions of coconut biomass into a single architecture, combining a macroscopic lignocellulosic support with an oxygen-functionalized carbonaceous phase. Spectroscopic, morphological, and elemental analyses supported the successive incorporation of the different components, including a decrease in the C/O mass ratio from 2.23 $\pm$ 0.44 to 0.77 $\pm$ 0.33. Furthermore, ATR-FTIR, TGA, and solid-state UV–Vis analyses demonstrated chemical modifications of the endocarp-derived carbon while confirming that OxCM remained distinguishable from conventional graphite-derived graphene oxide.

The resulting composite exhibited appreciable PQT adsorption under dark conditions, reaching 32.81 $\pm$ 2.64% after 6 h and 47.27 $\pm$ 2.85% after 72 h. Under direct solar irradiation, apparent PQT removal reached approximately 66.3% after 6 h, corresponding to a material-associated contribution of approximately 58.5% after accounting for the irradiated control. Comparison with the corresponding dark experiment yielded an additional irradiation-associated contribution of approximately 25.7 percentage points. However, this difference represents an operational estimate rather than a direct measure of photocatalytic degradation or mechanistic synergy. These findings demonstrate enhanced apparent PQT removal under solar irradiation, although the specific contributions of the individual material components remain unresolved.

The present findings constitute a proof-of-concept evaluation of the proposed hybrid architecture rather than a comprehensive assessment of its photocatalytic performance or technological feasibility. In particular, the UV–Vis measurements do not independently establish chemical degradation or mineralization, while the available structural and adsorption characterization does not fully resolve the relationships between material properties and removal mechanisms. Furthermore, solar irradiance was not quantified, and the experiments were performed in duplicate under nonoptimized conditions. Other relevant considerations include the stability of the incorporated phases, regeneration and reusability, performance in complex aqueous matrices, and the implications of the preparation procedure for potential scale-up. Although these aspects remain to be investigated, the results demonstrate the feasibility of integrating complementary coconut biomass fractions into a multifunctional material and provide a basis for evaluating the suitability of this architecture for further development.

Author Contributions: Conceptualization, N.G.C.-G.; A.G.-Q. and M.P.; methodology, N.G.C.-G. and A.G.-Q.; investigation, data curation, writing—review and editing, N.G.C.-G., A.G.-Q. and M.P.;

supervision, M.P.; and project administration, M.P.; funding acquisition, M.P. All authors have read and agreed to the published version of the manuscript.

Funding: This research was funded by the General Royalties' System of Colombia (SGR/DNP/Mindtech), grant number BPIN 2020000100261, the Ministry of Science, Technology and Innovation of Colombia (Minciencias), grant number project 8620-905-86033 (contract 80740-467-2021, CI:71320), and Universidad del Valle and Mindtech S.A.S., grant number MT-012025, C.I. 71408 (agreement MT-AFICAT-202501).

Data Availability Statement: Data available on request due to restrictions (further studies derived from this research are currently underway). Requests to access the datasets should be directed to corresponding authors.

Acknowledgments: The authors thank the Ministry of Science, Technology and Innovation of Colombia, General Royalties' System of Colombia, Universidad del Valle, Universidad de Córdoba and Mindtech S.A.S for the funds received. The authors give thanks to Hernán Valle from the Department of Chemistry, Universidad de Córdoba (Montería, Colombia), for supplying graphite-derived graphene oxide.

Conflicts of Interest: Authors Nazly G. Chate-Galvis and Angélica García-Quintero were employed by the company Mindtech S.A.S. The remaining authors declare that the research was conducted in the absence of any commercial or financial relationships that could be construed as potential conflicts of interest. The funder was not involved in the study design, collection, analysis, interpretation of data, the writing of this article or the decision to submit it for publication.

References

1. Chen, J.; Su, Y.; Lin, F.; Iqbal, M.; Mehmood, K.; Zhang, H.; Shi, D. Effect of paraquat on cytotoxicity involved in oxidative stress and inflammatory reaction: A review of mechanisms and ecological implications. *Ecotoxicol. Environ. Saf.* **2021**, *224*, 112711. [CrossRef]
2. Franco, D.S.P.; Georgin, J.; Lima, E.C.; Silva, L.F.O. Advances made in removing paraquat herbicide by adsorption technology: A review. *J. Water Process Eng.* **2022**, *49*, 102988. [CrossRef]
3. Tongur, T.; Ayranci, E. Adsorption and electrosorption of paraquat, diquat and difenzoquat from aqueous solutions onto activated carbon cloth as monitored by in-situ UV–visible spectroscopy. *J. Environ. Chem. Eng.* **2021**, *9*, 105566. [CrossRef]
4. Nasir, A.; Khalid, S.; Yasin, T.; Mazare, A. A review on the progress and future of TiO_2/graphene photocatalysts. *Energies* **2022**, *15*, 6248. [CrossRef]
5. Marien, C.B.D.; Le Pivert, M.; Azaïs, A.; M'Bra, I.C.; Drogui, P.; Dirany, A.; Robert, D. Kinetics and mechanism of Paraquat's degradation: UV-C photolysis vs UV-C photocatalysis with TiO_2/SiC foams. *J. Hazard. Mater.* **2019**, *370*, 164–171. [CrossRef]
6. Nguyen-Phan, T.-D.; Pham, V.H.; Shin, E.W.; Pham, H.-D.; Kim, S.; Chung, J.S.; Kim, E.J.; Hur, S.H. The role of graphene oxide content on the adsorption-enhanced photocatalysis of titanium dioxide/graphene oxide composites. *Chem. Eng. J.* **2011**, *170*, 226–232. [CrossRef]
7. Yunarti, R.T.; Safitri, T.N.; Dimonti, L.C.C.; Aulia, G.; Khalil, M.; Ridwan, M. Facile synthesis of composite between titania nanoparticles with highly exposed (001) facet and coconut shell-derived graphene oxide for photodegradation of methylene blue. *J. Phys. Chem. Solids* **2022**, *160*, 110357. [CrossRef]
8. Gonçalves, G.; Marques, P.A.A.P.; Pinto, R.J.B.; Trindade, T.; Neto, C.P. Surface modification of cellulosic fibres for multi-purpose TiO_2-based nanocomposites. *Compos. Sci. Technol.* **2009**, *69*, 1051–1056. [CrossRef]
9. Cunha, A.G.; Freire, C.S.R.; Silvestre, A.J.D.; Neto, C.P.; Gandini, A.; Belgacem, M.N.; Chaussy, D.; Beneventi, D. Preparation of highly hydrophobic and lipophobic cellulose fibers by a straightforward gas–solid reaction. *J. Colloid Interface Sci.* **2010**, *344*, 588–595. [CrossRef]
10. Palencia, M.; Chate, N.G.; García-Quintero, A. Obtaining micrometric-scale hollow fibers from wastes aged coir by oxidative chloro-sulfonation of lignin: $HClO/H_2SO_4$. *Bioresour. Technol. Rep.* **2024**, *25*, 101812. [CrossRef]
11. Sujiono, E.H.; Zurnansyah; Zabrian, D.; Dahlan, M.Y.; Amin, B.D.; Samnur; Agus, J. Graphene oxide based coconut shell waste: Synthesis by modified Hummers method and characterization. *Heliyon* **2020**, *6*, e04568. [CrossRef]
12. Hasan, K.M.F.; Horváth, P.G.; Bak, M.; Alpár, T. A state-of-the-art review on coir fiber-reinforced biocomposites. *RSC Adv.* **2021**, *11*, 10548–10571. [CrossRef]

13. Cunha, A.G.; Lundahl, M.; Ansari, M.F.; Johansson, L.-S.; Campbell, J.M.; Rojas, O.J. Surface structuring and water interactions of nanocellulose filaments modified with organosilanes toward wearable materials. *ACS Appl. Nano Mater.* **2018**, *1*, 5279–5288. [CrossRef]
14. Beaumont, M.; Bacher, M.; Opietnik, M.; Gindl-Altmutter, W.; Potthast, A.; Rosenau, T. A general aqueous silanization protocol to introduce vinyl, mercapto or azido functionalities onto cellulose fibers and nanocelluloses. *Molecules* **2018**, *23*, 1427. [CrossRef]
15. Abdelmouleh, M.; Boufi, S.; Belgacem, M.N.; Duarte, A.P.; Ben Salah, A.; Gandini, A. Modification of cellulosic fibres with functionalised silanes: Development of surface properties. *Int. J. Adhes. Adhes.* **2004**, *24*, 43–54. [CrossRef]
16. Castellano, M.; Gandini, A.; Fabbri, P.; Belgacem, M.N. Modification of cellulose fibres with organosilanes: Under what conditions does coupling occur? *J. Colloid Interface Sci.* **2004**, *273*, 505–511. [CrossRef]
17. Brusko, V.; Khannanov, A.; Rakhmatullin, A.; Dimiev, A.M. Unraveling the infrared spectrum of graphene oxide. *Carbon* **2024**, *229*, 119507. [CrossRef]
18. Eigler, S.; Dotzer, C.; Hof, F.; Bauer, W.; Hirsch, A. Sulfur species in graphene oxide. *Chem. Eur. J.* **2013**, *19*, 9490–9496. [CrossRef]
19. Farivar, F.; Lay Yap, P.; Karunagaran, R.U.; Losic, D. Thermogravimetric analysis (TGA) of graphene materials: Effect of particle size of graphene, graphene oxide and graphite on thermal parameters. *C* **2021**, *7*, 41. [CrossRef]
20. Kumar, N.; Srivastava, V.C. Simple synthesis of large graphene oxide sheets via electrochemical method coupled with oxidation process. *ACS Omega* **2018**, *3*, 10233–10242. [CrossRef]
21. Larena, A.; de la Orden, M.U.; Martínez Urreaga, J.M. Thermal and Fourier transform-infrared study of E-glass short-fiber functionalization with methylvinyldichlorosilane and vinyltrichlorosilane. *J. Colloid Interface Sci.* **1992**, *149*, 34–39. [CrossRef]
22. Tan, X.; Jiang, Y.; Peng, Q.; Subrova, T.; Saskova, J.; Wiener, J.; Venkataraman, M.; Militky, J.; Kejzlar, P.; Mahendran, A.R.; et al. Development and characterization of silane crosslinked cellulose/graphene oxide conductive hydrophobic membrane. *Cellulose* **2023**, *30*, 4561–4574. [CrossRef]
23. Toro, R.G.; Adel, A.M.; de Caro, T.; Brunetti, B.; Al-Shemy, M.T.; Caschera, D. A facile one-pot approach to the fabrication of nanocellulose–titanium dioxide nanocomposites with promising photocatalytic and antimicrobial activity. *Materials* **2022**, *15*, 5789. [CrossRef]
24. Sun, X.; Wang, K.; Shu, Y.; Zou, F.; Zhang, B.; Sun, G.; Uyama, H.; Wang, X. One-pot route towards active TiO_2-doped hierarchically porous cellulose: Highly efficient photocatalysts for methylene blue degradation. *Materials* **2017**, *10*, 373. [CrossRef]
25. Newbury, D.E.; Ritchie, N.W.M. Performing elemental microanalysis with high accuracy and high precision by scanning electron microscopy/silicon drift detector energy-dispersive X-ray spectrometry (SEM/SDD-EDS). *J. Mater. Sci.* **2015**, *50*, 493–518. [CrossRef]
26. Nguyen, C.; Tungtakanpoung, D.; Tra, V.T.; Kajitvichyanukul, P. Kinetic, isotherm and mechanism in paraquat removal by adsorption process using corn cob biochar produced from different pyrolysis conditions. *Case Stud. Chem. Environ. Eng.* **2022**, *6*, 100248. [CrossRef]
27. Dehghani, Z.; Sedghi-Asl, M.; Ghaedi, M.; Sabzehmeidani, M.M.; Adhami, E. Ultrasound-assisted adsorption of paraquat herbicide from aqueous solution by graphene oxide/mesoporous silica. *J. Environ. Chem. Eng.* **2021**, *9*, 105043. [CrossRef]
28. Moctezuma, E.; Leyva, E.; Monreal, E.; Villegas, N.; Infante, D. Photocatalytic degradation of the herbicide "Paraquat". *Chemosphere* **1999**, *39*, 511–517. [CrossRef]
29. Moradi, M.; Akbari Sene, R.; Rahmani, F.; Rezakazemi, M. Efficient photodegradation of paraquat herbicide over TiO_2-WO_3 heterojunction embedded in diatomite matrix and process optimization. *Environ. Sci. Pollut. Res.* **2023**, *30*, 99675–99693. [CrossRef]

Disclaimer/Publisher's Note: The statements, opinions and data contained in all publications are solely those of the individual author(s) and contributor(s) and not of MDPI and/or the editor(s). MDPI and/or the editor(s) disclaim responsibility for any injury to people or property resulting from any ideas, methods, instructions or products referred to in the content.